Soft Matter

ARTICLE TYPE

Cite this: DOI: 10.1039/xxxxxxxxxx

Theory of Polymer-Electrolyte-Composite Electroactuator Sensors with Flat or Volume-Filling Electrodes†

Zachary A. H. Goodwin,[a,b] and Alexei A. Kornyshev *[,b,c]

.

Received Date
Accepted Date

DOI: 10.1039/xxxxxxxxxx

www.rsc.org/journalname

In reverse actuation, a voltage/electrical-current signal can be generated from applying a mechanical force to an electroactuator. Such processes are of interest in touch sensing and soft robotics applications. We develop a classical density functional theory of reverse actuation for polymer-electrolyte-composite electroactuators, that treats mobile cations in the same spirit as forward actuation (curving in response to applied voltage). The proposed framework is applied to electroactuators with micro-structured porous electrodes (with cylindrical or slit pores) and flat electrodes, the dynamic response of which has to be modelled differently. Open- and short-circuit operation modes are investigated separately. A detailed analysis of the proposed theory indicates the preferred architectures for sensing, depending on the operation regimes.

1 Introduction

There is great interest in developing electroactuators for soft robots and touch sensors.[1–4] Amongst the most promising candidates for which are ionic polymer metal composites (IPMCs)[5–16] and composites made from hydrated ionomers with carbon-based electrodes.[3,4,17–26] Generally, electroactuators composed of polymer-electrolyte films, such as Nafion (where the proton has been replaced by a mobile bulky cation)[11–14] confined between two electrodes, curve in response to an applied voltage across the electrodes (forward actuation). Whereas when the electroactuator is curved, originating from an external mechanical force, an output voltage or transient current can be generated (reverse actuation). Both of which, forward and reverse actuation (see Fig. 1 for more details), involve the redistribution of the mobile cations and solvent.[27–40]

Since Ref. 13, where forward and reverse actuation was first described with a physics-based theory, there has been substantial research into developing more responsive (from an applied voltage) and sensitive (in terms of reverse actuation) electroactuators.[3–40] Advances in forward actuation have entailed the use of volume-filling electrodes[41–51] to increase the volumetric stress induced from the redistribution of ions. On the other hand, improvements to the sensitivity of reverse actuation has not been *a priori* obvious, although some experiments have indicated using ions of larger hydrated volumes in both flat and volume-filling electrodes.[31,33]

Nemat-Nasser and Li proposed a micromechanical description of reverse actuation.[13] In that theory, upon application of a force, open-circuit voltage was calculated from the assumption that the cations, in their local pockets of hydrated ionomer (enclosed by SO_3^- groups in Nafion, for example), would be displaced slightly from the equilibrium positions they would have occupied without an applied force. The displacement of cations relative to immobile anions forms dipoles throughout the ionomer; all of which are aligned, constructively interfering to create the open-circuit voltage. The theory was in good agreement with experiments,[13] but it required a detail knowledge of the ionomers structure.

Subsequently, Farinholt and Leo[31] suggested a reciprocity between forward and reverse actuation: both processes involve a direct proportionality between the induced stress and charge density. This conjecture permitted general, simple equations to be obtained under the operating condition of short-circuit, which were found to agree reasonably well with experiments.[31] The downfall of that approach, however, was the unknown parameter; that being, the proportionality constant between stress and charge density. Therefore, experimental data could be fitted but not predicted. Moreover, in the reported experiments it was found that the proportionality constant should depend on the volume of the mobile ion, but as mentioned in that paper the theoretical approach had no means to rationalise this observation.[31]

More recently, in Ref. 36 both open- and short-circuit characteristics have been derived from the so-called governing equations. There, sensing capabilities were introduced through the assump-

[a] *Department of Physics, CDT Theory and Simulation of Materials, Imperial College London, South Kensington Campus, London SW7 2AZ, UK.*
[b] *Department of Chemistry, Imperial College London, South Kensington Campus, London SW7 2AZ, UK.*
[c] *Thomas Young Centre for Theory and Simulation of Materials, Imperial College London, South Kensington Campus, London SW7 2AZ, UK.*

† Electronic Supplementary Information (ESI) available. See DOI: 10.1039/cXsm00000x/

* Corresponding author: a.kornyshev@imperial.ac.uk

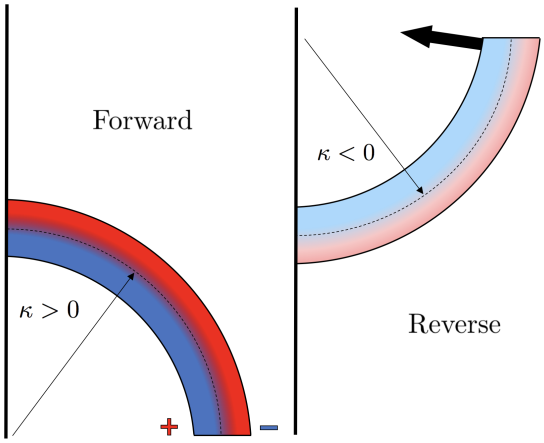


Fig. 1 Depiction of forward and reverse actuation. In forward actuation (left) a voltage is applied to the electrodes of the composite. The mobile ions (only cations here) in the ionomer redistribute, which causes stress in the vicinity of the electrodes. As shown, the upper electrode is polarised negatively (blue minus sign), such that cations (red region of actuator) distribute near the electrode to reside in the favourable electrostatic field; this leaves the region near the lower, positively polarised (red positive sign), electrode with a deficiency of cations (blue region of actuator). Electroactuators are partially flexible, and so the beam curves, with curvature κ (sign convention utilised here indicated), to relieve the stress due to such rearrangement of ions. For simplicity, considering narrow beams we assume it curves only in longitudinal direction, as shown. The curvature of such beam is defined as the inverse of its radius (i.e. twice its mean curvature).[52] Reverse actuation is when an applied force, depicted with a black arrow, curves the actuator and causes an electrical response in the electrodes. The distributions of ions depends on the system set up (open or short circuit).

tion that the immobile counterion concentration in the ionomer changes linearly with curvature, which resulted in the theory having no free parameters.[36] The obtained equation for open-circuit voltage (from the boundary condition of no current) was not directly related with the characteristics of the ionomer or mobile cation.[36,37] Experiments, however, have shown the generated signal depends on such characteristics.[31,33]

It is implicit to all descriptions of electroactuation that ions act in an analogous manner to defects in the theory of elasticity of solids.[51,53] When a voltage is applied to the electrodes, the mobile ions redistribute to reside in an energetically favourable electrostatic field.[11,13,14] The positions of the ions in the electrical double layer at the interface of the electrode are not favourable in terms of their elastic energy, however. This stressful region can cause the hydrated ionomer to expand.[11,12,51] In reverse actuation, modelling ions explicitly as defects has not yet been investigated. Here we bridge that gap.

The structure of the article is as follows. First, the general functional for reverse actuation is presented and discussed. Open-circuit voltage is obtained from the electroneutrality condition and its dependence on system parameters discussed. Thereafter, short-circuit characteristics are presented in the main text for flat electrodes and micro-structured electrodes with cylindrical pores (in Fig. 2 the studied electrode architectures are displayed). Following the theoretical analysis, stimulated by its results, we will discuss the best structure for reverse actuation depending on operating regimes.

2 Theory

To start we shall pedagogically outline the intimate connection between forward and reverse actuation. In forward actuation a voltage is applied to the electrodes. This causes the mobile cations to redistribute from the positively polarised electrode to the negatively polarised one. As a result, cation-depleted and cation-rich ionic space charges (electrical double layers)* form at the corresponding electrodes. The presence/absence of cations in the electrical double layers, which act as volumetric defects, causes stressful regions to develop in the ionomer; to partially relieve the elastically unfavourable domains, the flexible electroactuator bends.

Once the actuator is bent (from the applied voltage in this example), the distribution of ions and electrostatic potential distribution should have *characteristics of reverse actuation*. Therefore, both forward and reverse actuation electroactive responses exist when there is an applied voltage; and any theory developed for forward actuation must naturally contain the reverse actuation response.[11,12] It is interesting to note, and will become more apparent later, that in Refs. 11 and 12, where the case of forward actuation was solved self-consistently, the reverse actuation electroactive response was already contained within the developed forward actuation formalism.

If one imagines that something then holds the curved electroactuator in place and shorts the electrodes, it would be expected that most of the charge on the electrodes is quenched. Therefore, the majority of the accumulated charge in the electrical double layers is released. Hence, it should be clear that sensing is always a smaller effect (than forward actuation) because there is not a strong electrostatic driving force to redistribute the cations.

On the other hand, if the electrodes are under open-circuit conditions, then there is no net charge in the electrodes to screen. Therefore, as previously reported,[36] the hydrated ionomer does not break local electroneutrality anywhere, at least at equilibrium, when sensing in open-circuit.[13]

In the presented classical density functional formalism an external force is assumed to bend the actuator with constant curvature, κ, as depicted in Fig. 1; this is the only place where the external force is implicitly introduced into the theory. In contrast to forward actuation, there is no elastic energy penalty term, but otherwise the free energy functional remains the same.[11,12,51] For a specified curvature we intend to find the the electrostatic potential distribution, charge density distribution, surface charge density, net charge of an electrode and the transient electrical current.

The general free energy functional for reverse actuation, with bending as depicted in Fig. 1, can be approximated by

* In single mobile charge carrier materials,[54] such as Nafion, the positively charged double layer is formed by an excess of cations with a background of 'homogeneously' distributed SO_3^- groups, whereas the negatively charged electrical double layer comprises of and abundance of stationary SO_3^- groups, not compensated by cations.

This journal is © The Royal Society of Chemistry [year]

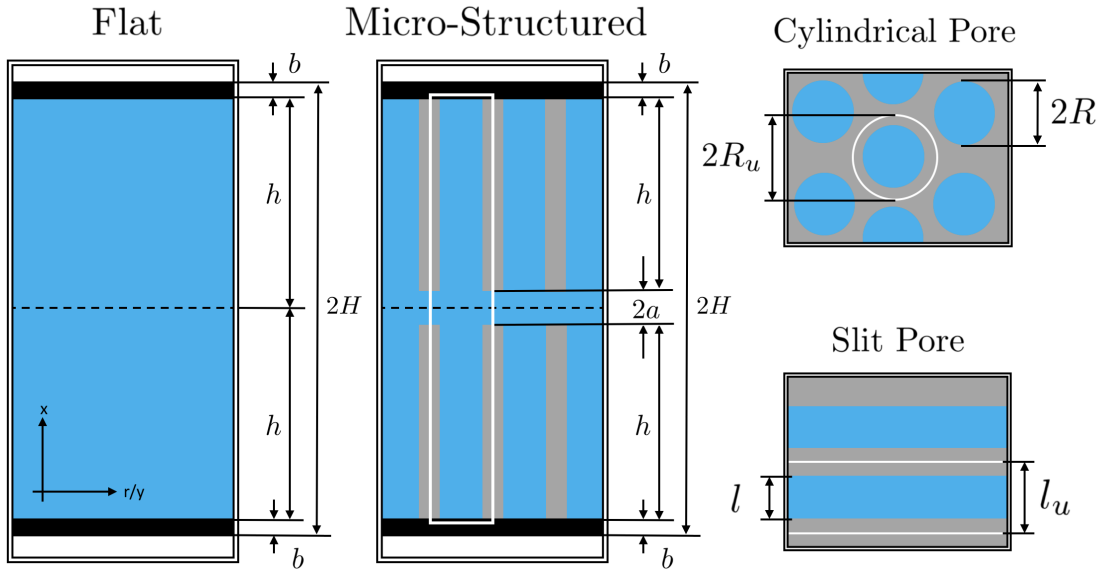


Fig. 2 Representation of the studied electrode architectures. Flat electrode electroactuators are depicted on the left. The blue region, of thickness $2h$, represents the hydrated ionomer with a single mobile cation, and the black regions represent the electrodes and casing. The general form of volume-filling micro-structured electrodes is depicted in the middle. The colour coding is the same as flat electrodes, with additional grey regions to illustrate the micro-structured electrodes which interpenetrate the ionomer. For micro-structured electrodes h refers to the length of the pores in the electrodes, and $2a$ is the thickness of the layer of the ionomer separating the two porous electrodes. On the right the two types of studied micro-structured electrodes, with cylindrical and slit pores, are sketched. The white lines in the micro-structured diagrams represent the 'unit cell'. The dashed black line indicates the neutral plane in the middle of the construction.

$$\mathcal{F} = \int d\mathbf{r}\Big[-\frac{\varepsilon}{8\pi}(\nabla\psi(\mathbf{r}))^2 + e\psi(\mathbf{r})\rho(\mathbf{r}) + k_BTg(\mathbf{r}) - Kv\rho(\mathbf{r})\kappa x\Big]. \quad (1)$$

The first two terms are electrostatic energy contributions (in Gaussian units throughout), where ε, $-\nabla\psi(\mathbf{r})$, e, $\psi(\mathbf{r})$ and $\rho(\mathbf{r}) = c_+(\mathbf{r}) - c_-(\mathbf{r})$ are the relative permittivity, electric field, elementary charge, electrostatic potential, and excess charge concentration, given by the cation concentration minus the anion concentration, respectively. The third term is the lattice-gas energy of a single mobile cation, where

$$g(\mathbf{r}) = c_+(\mathbf{r})\ln\left\{\frac{c_+(\mathbf{r})}{c_{max}}\right\} + (c_{max} - c_+(\mathbf{r}))\ln\left\{1 - \frac{c_+(\mathbf{r})}{c_{max}}\right\}, \quad (2)$$

with $c_+(\mathbf{r})$ and c_{max} denoting the local concentration and the maximal possible concentration of cations, respectively.[54†] The last term in Eq. (1) couples the excess charge concentration with the curvature of the electroactuator, where K and v are the bulk modulus[‡] and excess volume of an ion,[§] respectively.[11,12,51] From Eq. (1) it is clearly seen that the energy is lowered when cations redistribute from domains of the ionomer with negative strain to regions of positive strain.

Note that the employed functional is a local one which neglects correlations beyond the mean-field and it accounts for excluded volume effects through a simple lattice-gas term. There are, of course, differences in the results when the excluded volume effects are described using different approximations,[61] but these differences are minor at small voltages of the kind that we deal with in our paper.

In Ref. 31 an element of reciprocity between forward and reverse actuation was suggested. Here, this reciprocity appears because ions behave as volumetric defects in both forward and reverse actuation. This is why the term that couples curvature and excess charge concentration is the same in both free energy functionals.[11,12,51]

Minimising the free energy functional with respect to electrostatic potential

$$\frac{\delta\mathcal{F}}{\delta\psi} = 0 \quad (3)$$

yields the Poisson equation

$$\nabla^2\psi(\mathbf{r}) = -\frac{4\pi e}{\varepsilon}\rho(\mathbf{r}). \quad (4)$$

The number of anions in each infinitesimal thickness, dx, is assumed to be constant. This results in their dependence following $c_-(\mathbf{r}) = c_0/(1+\kappa x)$, where c_0 is the bulk concentration of anions.[36]

Minimising the functional with respect to $c_+(\mathbf{r})$ yields electrochemical potential of cations, $\bar{\mu}_+$. Chemical equilibrium requires

† Note that such approximations for taking into account excluded volume effects in concentrated electrolytes and ionic liquids has been used myriad times, being 'rediscovered' in many instances throughout the history of its use.[55–60]

‡ The bulk modulus is an effective parameter of the theory since electroactuators are composites.

§ Note that the excess volume of an ion is not necessarily equal to the volume of an ion since solvent can be replaced in the electrical double layer.

the electrochemical potential to equal the chemical potential in the neutral plane, $\mu_+(x=0)$. Solving the equality, $\bar{\mu}_+ = \mu_+$, permits the dependence of cation concentration on system parameters and variables to be obtained. Utilising the resulting equation in the excess charge concentration gives

$$\rho(\mathbf{r}) = -\frac{c_0}{(1+\kappa x)} \frac{(1-\gamma)\left[\exp\left\{\frac{e\psi(\mathbf{r})-Kv\kappa x}{k_BT}\right\} - 1 - \frac{\kappa x}{1-\gamma}\right]}{(1-\gamma)\exp\left\{\frac{e\psi(\mathbf{r})-Kv\kappa x}{k_BT}\right\} + \gamma}, \quad (5)$$

where $\gamma = c_0/c_{max}$ is the compacity of the mobile cations.

In Refs. 11 and 12, where a very similar Poisson equation was utilised, the problem of forward actuation was self-consistently solved. In that theory, which dealt with electroactuators with flat electrodes, it was found that most of the ionomer was in an electroneutral state ($\rho = 0$). As can be seen from Eq. (5), there must be a finite electrostatic potential in the bulk that linearly changes with displacement from the neutral plane ($x = 0$) for there to be electroneutrality. Such a dependence has been reported for reverse actuation multiple times.[31,36] As we shall outline here this linear electrostatic potential in the bulk gives rise to the sensing capabilities of electroactuators. Hence, that self-consistent theory was able to satisfy the requirement that a theory for forward actuation must also contain the reverse actuation response, although it was not noted at the time.[11,12]

2.1 Open-Circuit Voltage

Open-circuit sensing occurs under the idealisation of infinite resistance between the electrodes external connection. Under the electroneutral condition Eqs. (4)-(5) have a trivial solution, which affords for open-circuit voltage

$$\tilde{V} = \zeta\mathcal{K}\frac{x}{h}, \quad (6)$$

where $\tilde{V} = eV/k_BT$, $\zeta = Kv/k_BT$ and $\mathcal{K} = \kappa h$ are voltage in units of thermal voltage ($k_BT/e \approx 25$ meV at room temperature), dimensionless reverse actuator constant, and dimensionless curvature, respectively.

A positive electrostatic potential develops in the upper half of the electroactuator when there is a positive curvature (see Fig. 1), which prevents the cations from redistributing there and breaking electroneutrality. A similar linear relationship has been derived previously in Ref. 36, but with a different constant of proportionality between output voltage and curvature.

In the presented theory, open-circuit voltage increases with the stress caused by a volumetric defect. This relationship is quite intuitive: bulkier cations should have a greater preference for redistribution upon an applied mechanical force, owing to the correspondingly larger energy gain from moving a bulky cation from a region of compression to extension. It has been found in experiments[31,33] that the *sensing voltage* depends on the size of the mobile ion. This is in agreement with the presented theory. The stress also increases with the bulk modulus of the ionomer. Thus, bulky cations in 'strong' ionomers are preferable for open-circuit sensing.

2.2 Short-Circuit: Flat Electrodes

Short-circuit conditions occur when the external connections between electrodes have negligible electrical resistance. It shall henceforth be assumed that $1 \gg \kappa x$, such that $1 + \kappa x \approx 1$; note that it is simple to extend the analysis to include this contribution, but we do not do so here for simplicity.[36] The open-circuit analysis demonstrated, in accordance with previous literature,[13,33,36,37] that the voltage is extremely small, being fractions of thermal voltage for typical system parameters and variables. Hence, it is reasonable to linearise the Poisson equation, formally only possible provided γ is not close to 1, but giving the correct physical behaviour for the whole range of γ in the end, to afford the studied Helmholtz equation in dimensionless form

$$\frac{d^2\tilde{\psi}_f(\tilde{x})}{d\tilde{x}^2} = (1-\gamma)\tilde{\psi}_f(\tilde{x}), \quad (7)$$

where $\tilde{\psi}_f = u_f(\tilde{x}) - \zeta\mathcal{K}\tilde{x}/\tilde{h}$.[11,12] Here, $u_f(\tilde{x}) = e\psi_f(x)/k_BT$ is electrostatic potential in the units of thermal voltage; $\tilde{x} = x\kappa_D$, with $\kappa_D = \sqrt{4\pi e^2 c_0/k_BT\varepsilon}$ denoting the inverse Debye length; and $\tilde{h} = h\kappa_D$.

Solving the Helmholtz equation, with boundary conditions $\tilde{\psi}_f(0) = 0$ and $\psi_f(\pm\tilde{h}) = 0$,[31] yields for the electrostatic potential distribution

$$u_f(\tilde{x}) = \zeta\mathcal{K}\left[\frac{\tilde{x}}{\tilde{h}} - \frac{\sinh\{\sqrt{1-\gamma}\tilde{x}\}}{\sinh\{\sqrt{1-\gamma}\tilde{h}\}}\right]. \quad (8)$$

In Fig. 3a) an illustrative electrostatic distribution is shown for flat electrodes.

The form of the electrostatic potential distribution first appeared in Ref. 31, but the parameters in the equation are different. Indeed, here they depend on system specific properties and, in principle, practically all parameters are known without any fitting (although this will have to be verified by experiments). The only parameter that is not generally well known is the excess volume of an ion, but this should be approximately equal to the volume of the hydrated ion,[12] provided minimal displacement of solvent occurs (further theoretical development through the inclusion of explicit solvent could remove some ambiguity in the evaluation of the excess volume). Moreover, if the excess volume of cations are the same in forward and reverse actuation, the former can be used to determine the values of the parameters of Eq. (8).[12] This would be interesting to experimentally verify, and would cement the reciprocity between forward and reverse actuation.

It is evident that there are two contributions to the electrostatic potential distribution in Eq. (8). The first, as seen on the left inside the brackets, has a linear dependence on displacement from the neutral line ($x = 0$), as found in the previous section. Hence, a major fraction of the polymer-electrolyte membrane is electroneutral. The second term in the brackets comes from screening of electrode charge, and therefore it only contributes to the distribution in the electrical double layer regions.

An interesting feature of Eq. (8) is when $\gamma = 1$. Under this special case, the short-circuit electrostatic potential distribution recovers that of open-circuit, owing to ions not being able to move

This journal is © The Royal Society of Chemistry [year]

and form electrical double layers at the interface.

The excess charge concentration[¶] is given by

$$\tilde{\rho}_f(\tilde{x}) = (1-\gamma)\zeta\mathcal{K}\frac{\sinh\{\sqrt{1-\gamma}\tilde{x}\}}{\sinh\{\sqrt{1-\gamma}\tilde{h}\}}, \tag{9}$$

where $\tilde{\rho}_f(\tilde{x}) = \rho_f(\tilde{x})/c_0$. Analysing the excess charge concentration, an example of which is displayed in Fig. 3b), reveals that at the interfaces volumetric defects accumulate in regions of positive strain and deplete in domains of negative strain. For positive curvatures, cations redistribute from the lower electrode to reside in the vicinity of the upper electrode. This is the expected behaviour if one considers ions to behave as volumetric defects, since by redistributing mobile cations from regions of compression to extension the elastic energy can be partially relieved.

The dimensionless surface charge density of the electrode, $\tilde{\sigma} = -\tilde{\nabla}u|_{\tilde{h}}$,[‖] is then

$$\tilde{\sigma}_f = \zeta\mathcal{K}\left[\sqrt{1-\gamma}\coth\{\sqrt{1-\gamma}\tilde{h}\} - \frac{1}{\tilde{h}}\right]. \tag{10}$$

Since the thickness of the electroactuator, $2h$, is typically much longer than the Debye length ($\kappa_D h \gg 1$),[31] we can simplify the dimensionless surface charge density to

$$\tilde{\sigma}_f \approx \sqrt{1-\gamma}\zeta\mathcal{K}. \tag{11}$$

Provided the channels in the hydrated ionomer are large enough for continuous passage of cations from one electrode to the other and the mean height of roughness of the electrodes is significantly smaller than the separation between them (and that the thickness of the double layer is smaller than the height and the correlation length of roughness[62]), then the dynamics of electrode charging is determined by the migration of ions through the bulk ionomer with charging the electrical double layers occurring momentarily relative to the characteristic migration time (the latter assumption is warranted when h is much greater than the double layer thickness[54]). In Ref. 54 the dynamics of charging flat electrodes with single mobile charge carriers, in the high and low voltage limit, was explored. Such charging dynamics was the basis of the theory in Refs. 11 and 12 for the time-dependent characteristics of forward actuation. Since the voltages in reverse actuation are always extremely small, typically less than thermal voltage, it is sufficient to only utilise the low-voltage limit from Ref. 54.

As an idealisation here, it was assumed that the resistance of any external components is negligible. Such an approximation should be sufficient for sensing applications, but would not be adequate when the electrical response is performing work against a load in energy harvesting applications.

It is henceforth assumed that the time and spatial dependences are separable, and that there is initially a step change in the curvature of the electroactuator. Hence, the time-dependent charge of the upper electrode (situated at h) is given by

$$\tilde{Q}_f \approx -\sqrt{1-\gamma}\zeta\mathcal{K}\tilde{S}_f\left(1-\exp\left\{-\tilde{t}_f\right\}\right), \tag{12}$$

where $\tilde{Q}_f = Q_f/e$ is the number of accumulated charges, $\tilde{S}_f = S/4\pi l_B\lambda_D$ is the characteristic surface area scaling factor for flat electrodes, and the dimensionless time, $\tilde{t}_f = t/\tau_f$, depends on the characteristic decay time, τ_f, which is given by

$$\tau_f = \frac{h\lambda_D}{\sqrt{1-\gamma}D}\frac{S}{S_0}, \tag{13}$$

with λ_D, D, S and S_0 denoting the Debye length, diffusion coefficient of mobile cations, total surface area of one electrode and macroscopic surface area occupied by that electrode (note that $S > S_0$ in general because the electrodes are typically not perfect flat surface)[11,12], respectively. In Fig. 3c) the general curve for the accumulation of charge from a step change in curvature is displayed.

The corresponding dimensionless transient current, $\tilde{I} = d\tilde{Q}/d\tilde{t}$, from a step change in curvature is

$$\tilde{I}_f = -\sqrt{1-\gamma}\zeta\mathcal{K}\tilde{S}_f\exp\left\{-\tilde{t}_f\right\}. \tag{14}$$

In Fig. 3d) the dimensionless current scaled to the surface area factor is displayed.

2.3 Short-Circuit: Micro-Structured Electrodes with Cylindrical Pores

The structure of the electroactuator with micro-structured electrodes with cylindrical pores is depicted in Fig. 2. Since the resulting dimensionless equations for micro-structure electrodes with slit pores do not significantly differ, we analyse that structure in the Supplementary Information (SI)[†].

The assumptions formulated in the first paragraph of the previous section also apply here. It is further assumed that all edge effects, from the entrance and end of the pore, are negligible, such that the separating membrane is ignored (valid when $h >> a$). We employ a 'unit cell' concept for an average 'tandem pore' of the electroactuator, as seen in Fig. 2, by a cylinder which does not change with curvature of the beam (the assumption is valid when $1 >> \kappa x$).

The utilised dimensionless Helmholtz equation, valid when γ is not close to unit, in cylindrical coordinates is given by

$$\frac{1}{\tilde{r}}\frac{\partial}{\partial\tilde{r}}\left(\tilde{r}\frac{\partial\tilde{\psi}_c(\tilde{x},\tilde{r})}{\partial\tilde{r}}\right) + \frac{\partial^2\tilde{\psi}_c(\tilde{x},\tilde{r})}{\partial\tilde{x}^2} = (1-\gamma)\tilde{\psi}_c(\tilde{x},\tilde{r}). \tag{15}$$

where $\tilde{r} = \kappa_D r$ is the dimensionless radial coordinate and $\tilde{\psi}_c(\tilde{x},\tilde{r}) = u_c(\tilde{x},\tilde{r}) - \zeta\mathcal{K}\tilde{x}/\tilde{h}$.

It is assumed that the equation is separable, $\tilde{\psi}_c(\tilde{x},\tilde{r}) = X_c(\tilde{x})R_c(\tilde{r})$. The ordinary differential equation in the $\tilde{x}$ coordinate is taken to be

$$\frac{d^2X_c(\tilde{x})}{d\tilde{x}^2} = 0. \tag{16}$$

The solution of which is simply

¶ At linear response it is trivial to obtain excess charge concentration from $\rho_f = -k_BTc_0(1-\gamma)\tilde{\psi}_f$.

‖ In dimensional form the surface charge is given by $\sigma = e\tilde{\sigma}/4\pi l_B\lambda_D$, where $l_B = e^2/\varepsilon k_BT$ is the Bjerrum length and $\lambda_D = 1/\kappa_D$ is the Debye length.

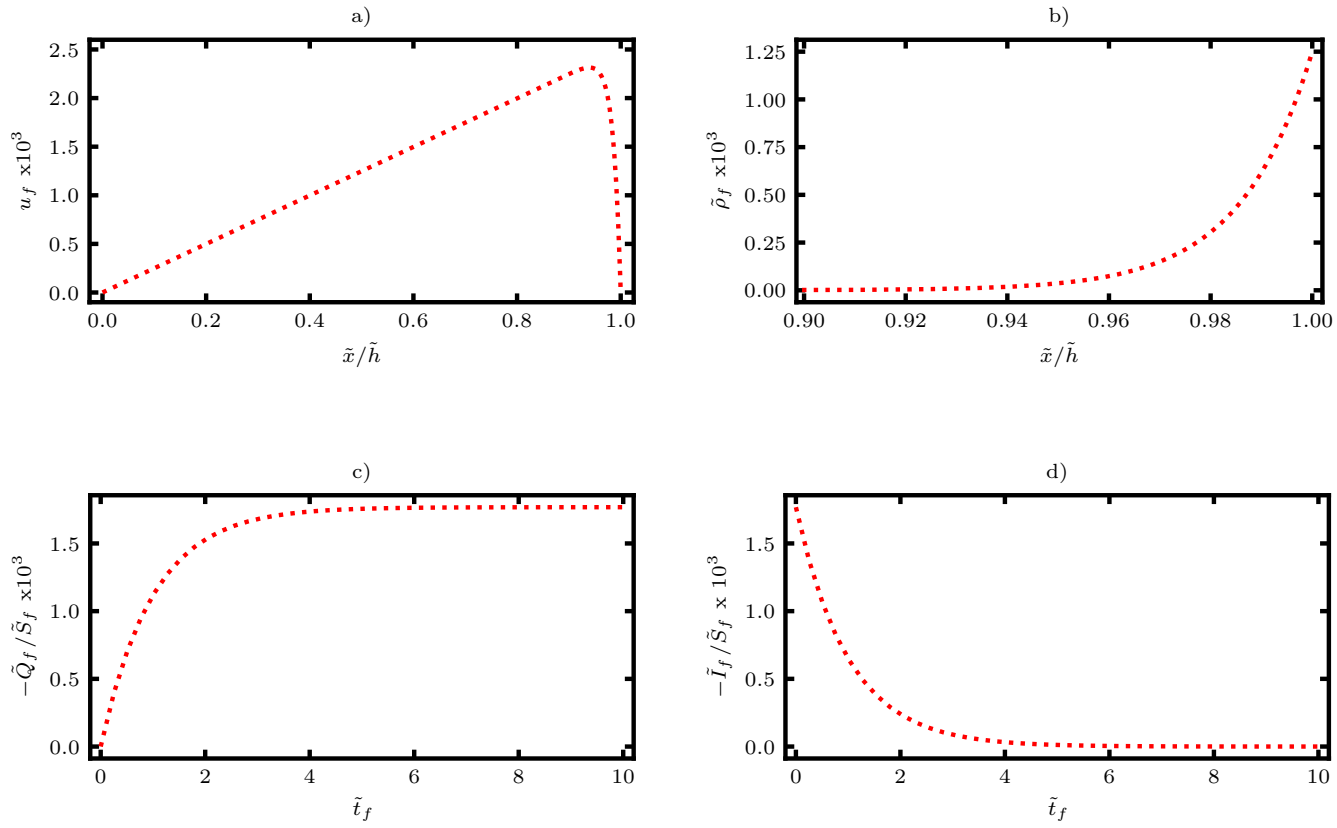


Fig. 3 Short-circuit characteristics for an electroactuator with flat electrodes. The parameters used were as follows $\mathcal{K} = 5$ x10^{-3}, $\tilde{h} = 100$ (note that this is significantly smaller than typical, which was chosen for illustrative effect. For typical systems, $\tilde{h}$ is of the order of 10^5), $\zeta = 0.5$ and $\gamma = 0.5$. a) - Distribution of electrostatic potential in units of thermal voltage as a function of dimensionless position in the ionomer. The linear relationship holds for the majority of the electroactuator, only near the electrodes does it deviate. b) - Excess charge concentration scaled to bulk concentration of cations as a function of position in the ionomer. Electroneutrality is only broken in the vicinity of the electrodes. c) - Dimensionless charge scaled to the surface area factor as a function of dimensionless time. d) - Dimensionless current scaled to the surface area factor as a function of time in the units of τ_f.

$$X_c = \frac{\zeta \mathcal{K} \tilde{x}}{\tilde{h}}. \tag{17}$$

The ordinary differential equation for the dimensionless radial coordinate is as follows

$$\frac{d^2 R_c(\tilde{r})}{d\tilde{r}^2} + \frac{1}{\tilde{r}} \frac{dR_c(\tilde{r})}{d\tilde{r}} = (1-\gamma) R_c(\tilde{r}). \tag{18}$$

The general solution of which is given by modified Bessel functions of the first and second kind. The modified Bessel function of the second kind must be discarded since it is not a physical solution for the problem at hand (in the center of the pore, the electrostatic potential distribution must be finite and equal to that of open-circuit). For the considered short-circuit case, the second boundary condition is simply, $u_c(\tilde{x}, \tilde{R}) = 0$.[31] Hence, the solution for dimensionless electrostatic potential inside a pore is

$$u_c(\tilde{x}, \tilde{r}) = \frac{\zeta \mathcal{K} \tilde{x}}{\tilde{h}} \left[1 - \frac{I_0(\sqrt{1-\gamma}\tilde{r})}{I_0(\sqrt{1-\gamma}\tilde{R})} \right], \tag{19}$$

where $\tilde{R} = \kappa_D R$ and I_0 is a modified Bessel function of the first kind.** As can be seen from Fig. 4a), the magnitude of the electrostatic potential increases with displacement from the neutral plane. Again, electrical double layers form only in the vicinity of the electrodes, leaving most of the hydrated ionomer inside the pore electroneutral.

The corresponding dimensionless excess charge concentration inside a pore is given by

$$\tilde{\rho}_c = (1-\gamma) \frac{\zeta \mathcal{K} \tilde{x}}{\tilde{h}} \frac{I_0(\sqrt{1-\gamma}\tilde{r})}{I_0(\sqrt{1-\gamma}\tilde{R})}. \tag{20}$$

As displayed in Fig. 4b) cations redistribute from the lower electrode to the upper one to form a cation-enriched electrical double layer there, leaving the lower electrode with a cation-depleted electrical double layer. It can also be seen that the extent of cation enrichment and depletion increases with displacement from the neutral plane.

Taking the derivative of Eq. (19) with respect to dimensionless

** The 0 refers to the order of the modified Bessel differential equation, namely Eq. (15). It is zeroth order because of the Laplace equation for $X_c(\tilde{x})$.

This journal is © The Royal Society of Chemistry [year]

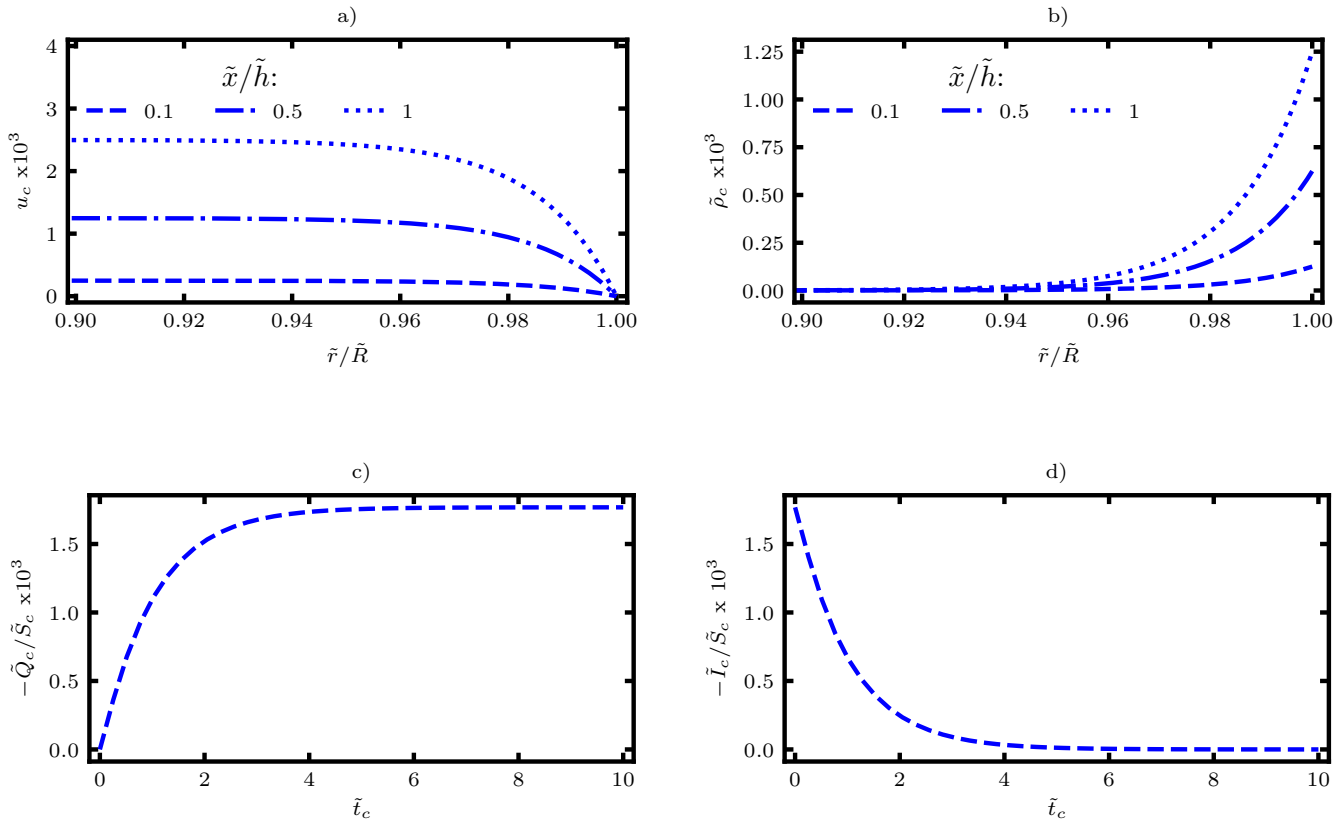


Fig. 4 Short-circuit characteristics for an electroactuator with micro-structured electrodes with cylindrical pores. The parameters used were $\mathcal{K} = 5$ x10^{-3}, $\tilde{R} = 100$, $\zeta = 0.5$ and $\gamma = 0.5$. a) - Electrostatic potential, scaled to thermal voltage, as a function of the radial coordinate in the pore for the indicated pore depths. Inside the pore, there is almost constant potential at each depth - deviations only occur near the electrode surface where space charges form. b) - Excess charge concentration, in units of bulk concentration of cations, as a function of radial coordinate in the pore for the indicated pore depths. c) - Charge, in units elementary charge, scaled to the surface area factor as a function of time in the units of τ_c. d) - Dimensionless current scaled to the surface area factor as a function dimensionless time.

coordinates yields the dimensionless electrostatic field. Evaluating the displacement field, $\mathcal{D} = \varepsilon\mathcal{E}$, at the upper electrode permits the dimensionless surface charge density of that pore to be obtained

$$\tilde{\sigma}_c(\tilde{x}) = \sqrt{1-\gamma}\frac{\zeta\mathcal{K}\tilde{x}}{\tilde{h}}\frac{I_1(\sqrt{1-\gamma}\tilde{R})}{I_0(\sqrt{1-\gamma}\tilde{R})}, \tag{21}$$

where I_1 is the modified Bessel function of the first kind of order 1.†† Since the pore radius is typically many times the Debye length, the dimensionless surface charge density simplifies to

$$\tilde{\sigma}_c(\tilde{x}) \approx \sqrt{1-\gamma}\frac{\zeta\mathcal{K}\tilde{x}}{\tilde{h}}. \tag{22}$$

The dynamical behaviour of charging a porous system, such as the discussed micro-structured electrodes, requires transmission line theory.[51,63] In which, the ions charging the electrical double layer move along the electrode surface, in the interior of the electrode pore. In doing so the electrical current moves through a series of resistors, off which capacitors can be charged as the ions migrate into the pore. Since the pore is finite in length, there is no current at the end of the pore, and only a transient current is observed.

Once again it is assumed that cations are much smaller than the channels of the elastomer in which they migrate, the resistance of external load is negligible and the surface charge density can be multiplied by a function of time and space that describes the dynamics of charging, as outlined in Ref. 51.

The total charge of one electrode is then approximately given by the charge per one pore multiplied by the number of them. Furthermore, since $h \gg a$ the integration can be approximately taken from 0 to $\tilde{h}$. Hence, the evolution of charge of the upper electrode can be approximated by

$$\tilde{Q}_c = -\sqrt{1-\gamma}\frac{2\zeta\mathcal{K}\tilde{S}_c}{\tilde{h}^2}\int_0^{\tilde{h}} d\tilde{x}\tilde{x}\phi_c(\tilde{x},\tilde{t}_c) \tag{23}$$

where $\tilde{S}_c = RhS_0/4\pi l_B\lambda_D R_u^2$ and the time-dependent function is given by[51]

†† This modified Bessel function comes from $I_1(z) = dI_0(z)/dz$.

$$\phi_c(\tilde{x},\tilde{t}_c) = 1 - \frac{4}{\pi}\sum_{n=0}^{\infty}\frac{(-)^n}{(2n+1)}\cdot$$
$$\cos\left[\left(n+\frac{1}{2}\right)\pi\left(1-\frac{\tilde{x}}{\tilde{h}}\right)\right]\exp\left\{-(2n+1)^2\tilde{t}_c\right\}; \quad (24)$$

the time is in units of τ_c, which is given by

$$\tau_c = \frac{8h^2C}{\pi^2R\Sigma}, \quad (25)$$

where C and Σ are the capacitance and ionic conductivity, respectively. It is sufficient to assume that the capacitance is constant, with a value of the Debye capacitance, since the equations have been solved at linear response. Evaluating the integral we obtained the net charge in the upper electrode

$$\tilde{Q}_c = -\sqrt{1-\gamma}\zeta\mathcal{K}\tilde{S}_c\left[1-\frac{32}{\pi^3}\sum_{n=0}^{\infty}\frac{(-)^n}{(2n+1)^3}\exp\left\{-(2n+1)^2\tilde{t}_c\right\}\right]. \quad (26)$$

In Fig. 4c) the general curve for charge accumulation of the upper electrode is displayed.

Taking the derivative of the above equation with respect to $\tilde{t}_c$ yields dimensionless current

$$\tilde{I}_c = -\sqrt{1-\gamma}\zeta\mathcal{K}\tilde{S}_c\left[\frac{32}{\pi^3}\sum_{n=0}^{\infty}\frac{(-)^n}{2n+1}\exp\left\{-(2n+1)^2\tilde{t}_c\right\}\right]. \quad (27)$$

An example curve for which is displayed in Fig. 4d). Remember, these dynamic equations have been derived with the assumption of no external resistance. Hence, deviations from these equations are expected when comparisons are made to experiments.[63]

3 Discussion

In dimensionless parameters and variables, there is clearly very similar equations for flat and micro-structured electrodes. To compare the different electroactuators, to reveal which type is most suited for sensing, the equations must be cast back into dimensional form. Structural parameters, such as our h and R, and alike, will always vary over the system. So hereafter, all corresponding notations will be considered averaged of the sample.

For open-circuit voltage the describing equations are

$$V_f = 2\frac{Kv}{e}h\kappa, \quad (28a)$$

$$V_c = 2\frac{Kv}{e}a\kappa, \quad (28b)$$

for flat electrodes and micro-structured electrodes with cylindrical pores, respectively. It has been found that the *sensing voltage*, Kv/e, is of the order of 10^{-1}-10^3 times thermal voltage.[12] This is in reasonable agreement with range reported in experiments, where open-circuit voltage is often found to be of the order of mV and increases linearly with the strain.[13,33] Moreover, experiments have found that the electroactive response of reverse actuation dependence on the volume of the mobile cations.[31,33] The above equations clearly have such dependence, which is in contrast to previously derived open-circuit equations for voltage.[36,37]

Which type of electroactuator is better for open-circuit sensing? For the same average curvature and overall device thickness ($2H$), it is evident that flat electrodes are preferable. This is because h is larger for flat electrodes than a is for micro-structured electrodes. Hence, flat electrode electroactuators with large distances between the electrodes are optimal for open-circuit sensing. It is advantageous to sense in open-circuit because of the one-to-one correspondence between curvature and voltage, and because the electroactuator does not have to be in a dynamic state to obtain information on its curvature.

For short-circuit sensing it is preferable to measure the charge accumulated, rather than the current, because of the one-to-one correspondence between charge accumulated and curvature at long times, in a static state. Therefore, we shall further discuss the accumulated charge for short-circuit sensing.

What type of electroactuator is better for short-circuit sensing? Since the net charge accumulated scales with the surface area of the electrodes, it is somewhat trivial to understand that, for the same device size, the micro-structured electrodes should be substantially more sensitive than flat electrodes. The ratio of the charge accumulated in micro-structured electrodes to that of flat electrodes is

$$\frac{Q_c}{Q_f} = \frac{S_0}{S}p_c\frac{h}{R}. \quad (29)$$

Both S_0/S and p_c are less than 1, but they are not necessarily substantially so. Since $h \gg R$, the charge accumulated is, in fact, significantly larger for micro-structured electrodes with cylindrical pores. In the SI[†] the ratio of the charge accumulated in micro-structured electrodes with slit pores is compared to flat electrodes, where an analogous expression is found. Therefore, micro-structured electrodes should be used for sensing in short-circuit .

4 Conclusions

To summarise, a classical density functional theory formalism was developed for the description of reverse actuation, in which ions are modelled as volumetric defects. We found simple, analytical formula for the open-circuit voltage, and short-circuit surface charge density, accumulated charge and transient current from a step change in curvature. All measurable responses, voltage, charge and current, were found to linearly increase with the volume of the defect and the thickness of the electroactuator, independent of the type of the electroactuator. It was found that flat electrode electroactuators are preferable for open-circuit sensing, but micro-structured electrodes are advantageous for short-circuit sensing.

5 Acknowledgements

We are grateful for discussions with Professor M. Eikerling and Professor H. Löwen that stimulated this work. ZG was supported through a studentship in the Centre for Doctoral Training

This journal is © The Royal Society of Chemistry [year]

on Theory and Simulation of Materials at Imperial College London funded by the EPSRC (EP/L015579/1) and from the Thomas Young Centre under grant number TYC-101.

6 Conflict of Interest

The authors have no conflict of interest.

References

1 T. Mirfakhrai, J. D. W. Madden and R. H. Baughman, *Mater. Today*, 2007, **10**, 30–38.

2 L. Hines, K. Petersen, G. Z. Lum and M. Sitti, *Adv. Mater.*, 2017, **29**, 1603483.

3 L. Kong and W. Chen, *Adv. Mater.*, 2014, **26**, 1025–1043.

4 U. Kosidlo, M. O. M. Micusík, G. Ćirić-Marjanović, H. Randriamahazaka, T. Wallmersperger, A. Aabloo, I. Kolaric and T. Bauernhansl, *Soft Matter. Struct.*, 2013, **22**, 104022.

5 Q. He, X. Yang, Z. Wang, J. Zhao, M. Yu, Z. Hu and Z. Dai, *J. Bionic. Eng.*, 2017, **14**, 567–578.

6 S. V. Anand, K. Arvind, P. Bharath and D. R. Mahapatra, *Smart Mater. Struct.*, 2010, **19**, 045026.

7 D. Schicker and T. Wallmersperger, *J. Appl. Phys.*, 2013, **114**, 163709.

8 S. Nemat-Nasser, *J. Appl. Phys.*, 2002, **92**, 2899–2915.

9 J. D. Davidson and N. C. Goulbourne, *J. Appl. Phys.*, 2011, **109**, 084901.

10 C. Jo, D. Pugal, I.-K. Oh, K. J. Kim and K. Asaka, *Prog. Polym. Sci.*, 2013, **38**, 1037–1066.

11 A. A. Lee, R. H. Colby and A. A. Kornyshev, *J. Phys.: Condens. Matter*, 2013, **25**, 082203.

12 A. A. Lee, R. H. Colby and A. A. Kornyshev, *Soft Matter*, 2013, **9**, 3767–3776.

13 S. Nemat-Nasser and J. Y. Li, *J. Appl. Phys.*, 2000, **87**, 3321–3331.

14 T. Wallmersperger, A. Horstmann, B. Kröplin and D. J. Leo, *J. Intell. Mater. Syst. Struct.*, 2009, **20**, 741–750.

15 Y. Cha and M. Porfiri, *J. Mechan. Phys. Solids*, 2014, **71**, 156–178.

16 J. Arumugam, A. Srinivasa and J. Reddy, *Compos. Struct.*, 2013, **106**, 461–469.

17 I.-W. P. Chen, M.-C. Yang, C.-H. Yang, D.-X. Zhong, M.-C. Hsu and Y. Chen, *ACS Appl. Mater. Interfaces*, 2017, **9**, 5550–5555.

18 S. Liu, Y. Liu, H. Cebeci, R. G. de Villoria, J.-H. Lin, B. L. Wardle and Q. M. Zhang, *Adv. Funct. Mater*, 2010, **20**, 3266–3271.

19 V. Palmre, E. Lust, A. Jänes, M. Koel, A.-L. Peikolainen, J. Torop, U. Johanson and A. Aabloo, *J. Mater. Chem.*, 2011, **21**, 2577–2583.

20 R. H. Baughman, C. Cui, A. A. Zakhidov, Z. Iqbal, J. N. Barisci, G. M. Spinks, G. G. Wallace, A. Mazzoldi, D. D. Rossi, A. G. Rinzler, O. Jaschinski, S. Roth and M. Kertesz, *Science*, 1999, **284**, 1340–1344.

21 Y. Luo and X. Yu, *Eur. Polym. J.*, 2016, **82**, 290–299.

22 I. A. Levitsky, P. Kanelos and W. B. Euler, *J. Chem. Phys.*, 2004, **121**, 1058–1065.

23 M. Yu, Q. He, D. Yu, X. Zhang, A. Ji, H. Zhang, C. Guo and Z. Dai, *Appl. Phys. Lett.*, 2012, **101**, 163701.

24 N. Terasawa, *RSC Adv.*, 2017, **7**, 2443–449.

25 V. Palmre, D. Brandell, U. Mäeorg, J. Torop, O. Volobujeva, A. Punning, U. Johanson, M. Kruusmaa and A. Aabloo, *Smart Mater. Struct.*, 2009, **18**, 095028.

26 S. N. S, A. Punning, U. Johanson and A. Aabloo, *J. Appl. Phys.*, 2018, **123**, 014502.

27 M. Aureli, C. Prince, M. Porfiri and S. D. Peterson, *Smart Mater. Struct.*, 2010, **19**, 015003.

28 A. Giacomello and M. Porfiri, *J. Appl. Phys.*, 2011, **109**, 084903.

29 J. Brufau-Penella, M. Puig-Vidal, P. Giannone, S. Graziani and S. Strazzeri, *Smart Mater. Struct.*, 2008, **17**, 015009.

30 Y. Cha, L. Shen and M. Porfiri, *Smart Mater. Struct.*, 2013, **22**, 055027.

31 K. Farinholt and D. J. Leo, *Mechanics of Materials*, 2004, **36**, 421–433.

32 M. Aureli, C. Prince, M. Porfiri and S. D. Peterson, *Smart Mater. Struct.*, 2010, **19**, 015003.

33 S. Han, J. Zhao, D. Wang, C. Lua and W. Chen, *J. Mater. Chem. B*, 2017, **5**, 7126–7132.

34 Y. Bahramzadeh and M. Shahinpoor, *Smart Mater. Struct.*, 2011, **20**, 094011.

35 Z. Chen, X. Tan, A. Will and C. Ziel, *Smart Mater. Struct.*, 2007, **16**, 1477–1488.

36 Y. Cha, F. Cellini and M. Porfiri, *Phys. Rev. E*, 2013, **88**, 062603.

37 YoungsuCha and MaurizioPorfiri, *J. Mech. Phys. Solids*, 2014, **71**, 156–178.

38 M. Aureli and M. Porfiri, *Continuum Mech. Thermodyn.*, 2013, **25**, 273–310.

39 Y. Cha, M. Verotti, H. Walcott, S. D. Peterson and M. Porfiri, *Bioinspir. Biomim.*, 2013, **8**, 036003.

40 A. Giacomello and M. Porfiri, *J. Appl. Phys.*, 2011, **109**, 084903.

41 P. M. Biesheuvel and M. Z. Bazant, *Phys. Rev. E*, 2010, **81**, 031502.

42 K. Mukai, K. Asaka, K. Kiyohara, T. Sugino, I. Takeuchi, T. Fukushima and T. Aidab, *Electrochemi. Acta.*, 2008, **53**, 5555–5562.

43 K. Kruusamäe, T. Sugino and K. Asaka, *J. Appl. Phys.*, 2015, **118**, 014502.

44 B. J. Akle, W. Habchi, T. Wallmersperger, E. J. Akle and D. J. Leo, *J. Appl. Phys.*, 2011, **109**, 074509.

45 B. J. Akle and D. J. Leo, *Smart Mater. Struct.*, 2007, **16**, 1348–1360.

46 B. J. Akle and D. J. Leo, *Smart Mater. Struct.*, 2012, **21**, 105034.

47 B. Akle, S. Nawshin and D. Leo, *Smart Mater. Struct.*, 2007, **16**, S256–S261.

48 O. Kim, T. J. Shin and M. J. Park, *Nat. Commun.*, 2013, **4**, 2208.

49 Y. Cha, M. Verotti, H. Walcott, S. D. Peterson and M. Porfiri,

Bioinspir. Biomim., 2013, **8**, 036003.
50 L. Chang, K. Asaka, Z. Zhu, Y. Wang, H. Chen and D. Li, *J. Appl. Phys.*, 2014, **115**, 244901.
51 Z. A. H. Goodwin, M. Eikerling, H. Löwen and A. A. Kornyshev, *Smart Mater. Struct.*, 2018, **27**, 075056.
52 L. D. Landau and E. M. Lifschitz, *Theory of Elasticity*, Pergamon Press, 3rd edn, 1986.
53 B. A. Bilby, *Proc. Phys. Soc. A*, 1950, **63**, 191–200.
54 A. A. Kornyshev and M. A. Vorotyntsev, *Electrochim. Acta.*, 1981, **26**, 303–323.
55 M. Eigen and E. Wicke, *J. Phys. Chem.*, 1954, **58**, 702–714.
56 M. Z. B. ansd Mustafa Sabri Kilic, B. D. Storey and A. Ajdari, *Adv. Colloid Interface Sci.*, 2009, **152**, 48–88.
57 J. J. Bikerman, *Philos. Mag.*, 1942, **33**, 384–397.
58 A. A. Kornyshev, *J. Phys. Chem. B*, 2007, **111**, 5545–5557.
59 V. Kralj-Iglic and A. Iglic, *J. Phys. II*, 1996, **6**, 447–491.
60 I. Borukhov, D. Andelman and H. Orland, *Phys. ReV. Lett.*, 1997, **79**, 435–438.
61 D. Frydel and Y. Levin, *J. Chem. Phys.*, 2012, **137**, 164703.
62 L. I. Daikhin, A. A. Kornyshev and M. Urbakh, *Phys. Rev. E*, 1996, **53**, 6192–6199.
63 A. A. Kornyshev, R. M. Twidale and A. B. Kolomeisky, *J. Phys. Chem. C*, 2017, **121**, 7584–7595.

This journal is © The Royal Society of Chemistry [year]